Continuum Mechanics Meets Echocardiographic Imaging: Investigation on the Principal Strain Lines in Human Left Ventricle

A. Evangelista, S. Gabriele, P. Nardinocchi, P. Piras, P.E. Puddu, L. Teresi, C. Torromeo and V. Varano

Abstract We present recent investigations on the state of strain in human left ventricle based on the synergy between continuum mechanics and echocardiographic imaging. When data from three-dimensional Speckle Tracking Echocardiography are available, special strain directions can be detected on the epicardial and endocardial surfaces, which are well-known in continuum mechanics as principal strain lines (PSLs), further classified into primary and secondary strain lines. An appropriate investigation on PSLs can help to identify lines where strains are largest as primary and smallest as secondary. As PSLs change when cardiac diseases appear, the challenge is that the analysis may allow for the identification of new indicators of cardiac function.

P. Nardinocchi (✉) · P. Piras
Dipartimento di Ingegneria Strutturale e Geotecnica, Sapienza—Università di Roma,
Rome, Italy
e-mail: paola.nardinocchi@uniroma1.it

A. Evangelista
Ospedale San Giovanni Calibita Fatebenefratelli-Isola Tiberina, Rome, Italy

S. Gabriele · V. Varano
Dipartimento di Architettura, LaMS—Modeling & Simulation Lab,
Università Roma Tre, Rome, Italy

P. Piras
Dipartimento di Scienze, Università Roma Tre, Rome, Italy

Center for Evolutionary Ecology, Università Roma Tre, Rome, Italy

P. E. Puddu · C. Torromeo
Dipartimento di Scienze Cardiovascolari, Respiratorie, Nefrologiche, Anestesiologiche,
Sapienza Università di Roma, Rome, Italy

L. Teresi
Dipartimento di Matematica e Fisica, LaMS—Modeling & Simulation Lab,
Università Roma Tre, Rome, Italy

1 Introduction

The heart is a specialised muscle that contracts regularly and pumps blood to the body and the lungs. The center of the pumping function are the ventricles; due to the higher pressures involved, the left ventricle (LV) is especially studied. On a simplistic level, LV is a closed chamber, whose thick walls are composed of muscle fibres. It is the *contraction* originated in the muscles that translates into pressure and/or volume changes of the chamber. Moreover, the helicoidal fibres make relevant the torsion of the chamber with respect to the longitudinal axis due to both pressure changes and muscle contraction. The LV cycle may be schematized as the sequence of four steps: filling-the *diastolic* phase; isovolumetric contraction; ejection-the *systolic* phase; isovolumetric relaxation [1].

During the cycle, both pressure and volume vary in time, and a quite useful determinant of the cardiac performance is the plot representing the pressure-volume relationship in the LV during the entire cycle, that is, the PV loop; some of the many clues contained in the plot (see Fig. 1) are briefly summarized in the following. Point 1 defines the end of the diastolic phase and is characterized by the end-diastolic volume (EDV) and pressure (EDP); at this point the mitral valve closes and cardiac muscle starts to *contract* in order to increase the blood pressure. At point 2 the systolic phase begins: the aortic valve opens and blood is ejected outside the LV; muscle keeps on contracting in order to further the ejection, while volume decreases to a minimum. Point 3 defines the end of the systolic phase, and is characterized by the end-systolic volume (ESV) and pressure (ESP); starting from here, LV undergoes an isovolumic *relaxation* until point 4, where mitral valve opens and filling begins.

Fig. 1 Cartoon sketching the phases of the cardiac cycle of a normal human subject. *1* Mitral valve closes; isovolumetric contraction. *2* Aortic valve opens; ejection. *3* Aortic valve closes; relaxation. *4* Mitral valve opens, filling. The green area represents the stroke work
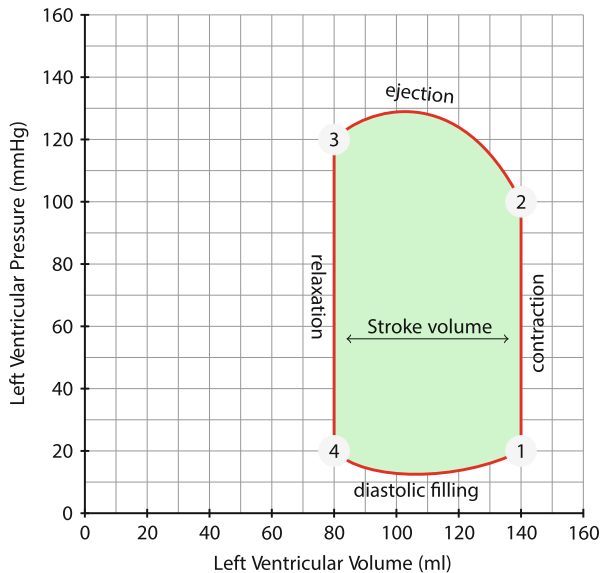
During the filling phase, muscle keeps on relaxing in order to accomodate a large increase in blood volume, while maintaining the pressure at a quite low level. Filling is completed at point 1. The difference between maximum and minimum volume is called stroke volume (SV): $SV := EDV - ESV$. From a mechanical point of view, the most intense work is performed along the pattern from point 2 to point 3, that is, along the systolic phase, when pressures are high and muscle contraction too. Typically, critical behaviors of the ventricular function are evidenced in this phase, and mechanics can suggest which are good indicators of cardiac function. A relevant condition about these indicators is the possibility to catch them through noninvasive analyses.

A well-known example is ventricular torsion [23]. The role played by the LV torsional rotation with respect to LV ejection and filling was only recently recognized by application of speckle tacking echocardiography, whose output includes, among the other things, the pattern of ventricular torsion along the cardiac cycle [4, 5, 10–12, 16]. As ventricular torsion is altered when a few pathologies are present (see [3, 13, 18, 22, 24, 28]), it can be used as an indicator of cardiac function which can be noninvasively investigated through 3-dimensional speckle tracking echocardiography (3DSTE).

Detection of principal strain lines in LV may emerge as another possible non-invasive tool to discriminate among different LVs as well as a tool that can help clinicians to identify cardiac diseases at the early stages. On the other hand, and differently from ventricular torsion, PSLs are not delivered as output by 3DSTE devices, and a post-processing analysis of 3DSTE data is needed to identify them, based on concepts borrowed from continuum mechanics. In [17, 20], it was initially proposed to look at PSLs to identify muscle fiber architecture on the endocardial surface. Therein, the echocardiographic analysis was limited to the endocardial surface, and it was noted as due to the high contractions suffered by muscle fibres along the systolic phase, PSLs may well determine just muscle fiber directions. Successively, in [8] an accurate protocol of measurement of PSLs was proposed, tested, and succesfully verified through a computational model. The conclusions of this last work were partially in contrast with the ones in [20]. It was demonstrated, firstly, that on the endocardial surface of healthy LVs, primary strain lines identify circumferential material directions; secondly, that on the epicardial surface primary strain lines are similar to muscle fiber directions. In [6, 8, 9], a comparison between a real human LV and a corresponding model was implemented by the same Authors; the conclusions of [8] were confirmed, and made precise through a statistical analysis involving real and computational data.

What is emerging, even if further investigations are needed, is that endocardial PSLs coincide with circumferential material lines, due to the relevant stiffening effect of the circumferential material lines when high pressures are involved, as it occurs along the systolic phase, and to the capacity of the same material fibers to contrast the LV dilation. It would mean that these visible functional strain lines are related to the capacity of elastic response of the cardiac tissue to the high systolic pressure, and that it might be important to follow this pattern when, due to pathological conditions, this capacity is missing.

2 Continuum Cardio-Mechanics

Typically, when mechanics is applied to biology, it is named biomechanics; we use cardio-mechanics to mean that specific branch of mechanics which has been successfully applied to the analysis and investigation of the cardiovascular system, whose center is the heart pump. Discuss the contribution of cardio-mechanics to clinics is beyond our aims (refer to [7] for extended references); we only aim to shortly discuss two different approaches of mechanics to clinics, with specific reference to the heart pump.

The first approach is based on the continuum analysis of the heart, aimed to model the cardiac activity. It starts from the construction of anatomical models of the heart and of constitutive model describing the passive and active material response of cardiac tissues. Electromechanical interaction are sometimes accounted for, if one has interest to also investigate cardiac electrophysiology. Typically, these models are implemented within a finite element code. Critical points are the constitutive models of the tissue, being cardiac tissue highly non homogeneous and contracting, due to an electrophysiological stimulus, and anatomical data about muscle architecture, which strongly influences the mechanical performances of the heart [14, 15, 27]. Once the model is complete, specific cardiac diseases can be included within the modeling, and the consequences on the heart activity studied. Typical examples are given by the investigations on the heart remodeling due to left anterior descending artery occlusion, to ventricular hypertrophy, to aortic stenosis, well discussed in literature [10, 18, 24]. Likewise, the model can be improved to account consequences of an infarct in different places of the left ventricular walls, with the aim of studying the ability of the pump to get on or not its work [13].

Here, we are more interested in the second approach, which starts from an analysis of real data extracted from the heart through appropriate tools such as Magnetic Risonance Image (MRI) and 3DSTE. Of course, such data are only concerning heart kinematics, and say nothing about stresses within heart walls. However, as it is recently shown, an accurate and careful analysis of real data allows to deeply investigate on heart. Let us note that the interest in in-vivo myocardial deformation dates back to ′80; in [26], the normal in-vivo three-dimensional finite strains were studied in dogs, through the application of appropriate markers whose coordinated were followed along the cardiac cycle through high-speed biplane cineradiography. Of course, the analysis was highly invasive. The recent techniques of visualization realized by 3DSTE make possible follow the coordinates of natural markers, automatically identified by the device, appropriately supported by an operator.

A typical example of the outcomes of a deep analysis on 3DSTE real data comes from PSLs, which are the core of this contribution. In mechanics, it is well-known that stresses and strains within a body are limited above and below by their principal counterparts; this allows for the discussion and verification of the mechanical state of that body. Moreover, the principal stress and strain lines (which are the same only when special symmetry conditions are verified) determine the directions where the largest strains and/or stresses are to be expected. Due to these characteristics, the mechanics of fiber-reinforced bodies are often based on the detection of the principal

strain lines and, wherever needed, fiber architecture is conceived in order to make the fiber lines coincide with the PSLs. Fibers make a tissue highly anisotropic; hence, principal strain and stress lines may be distinct. Whereas principal strains can be measured starting with the analysis of tissue motion, being only dependent on the three-dimensional strain state of the tissue, principal stresses can only be inferred. Thus, the PSL have a predominant role where the analysis of the mechanics of a body is concerned, and can reveal which are the lines where largest strains are expected, and how they change when diseases occur.

Key point is the evaluation at any place within the body of the nonlinear strain tensor $\mathbf{C}$, whose eigenpairs (eigenvalues-eigenvectors) deliver principal strains and PSLs, respectively. Fixed a body, identified with the region $\mathcal{B}$ of the three-dimensional Euclidean space $\mathcal{E}$ it occupies at a time t_o denoted as reference configuration of the body, we are interested in following the motion of the body at any time $t \in \mathcal{I} \subset \mathcal{R}$, with the time interval $\mathcal{I}$ identifying the duration of a human cardiac cycle (hence, different from subject to subject, as it is discussed later). The displacement field $\mathbf{u}$, that is a map from $\mathcal{B} \times \mathcal{T} \rightarrow \mathcal{V} = T\mathcal{E}$, delivers at any time and for any point $y \in \mathcal{B}$ the position $p(y, t)$ of that point at that time: $p(y, t) = y + \mathbf{u}(y, t)$. Strains are related to displacement gradients within the body; precisely, it can be shown as, introduced the deformation gradient $\mathbf{F} = \nabla p = \mathbf{I} + \nabla \mathbf{u}$, the nonlinear Cauchy-Green strain tensor is

$$\mathbf{C} = \mathbf{F}^T \mathbf{F} = \mathbf{I} + \nabla \mathbf{u} + \nabla \mathbf{u}^T + \nabla \mathbf{u}^T \nabla \mathbf{u}, \qquad (1)$$

being $\mathbf{I}$ the identity tensor in $\mathcal{V}$. In general, $\mathbf{C}$ is a three-dimensional tensor, describing the strain state at any point y and time t of the body. If there is within the body a distinguished surface $\mathcal{S}$, whose unit normal field is described by the unit vector field $\mathbf{n}$, the corresponding surface strain tensor $\hat{\mathbf{C}}$ can be obtained through a preliminary projection of $\mathbf{C}$ onto that surface. The projector $\mathbf{P} = \mathbf{I} - \mathbf{n} \otimes \mathbf{n}$, leads to the following definition:

$$\hat{\mathbf{C}} = \mathbf{PCP}. \qquad (2)$$

It is expected that $\hat{\mathbf{C}}$ will represent a plane strain state, hence, that it will have a zero eigenvalue corresponding to the eigenvector $\mathbf{n}$. The primary strain lines on the surface will be the streamlines of the eigenvector $\mathbf{c}_2$, which lies on the surface and corresponds to the smallest non-zero eigenvalues; the secondary strain lines are the streamlines corresponding to the eigenvector $\mathbf{c}_3$. Of course, when the strain tensor $\mathbf{C}$ is ab initio evaluated from surface deformation gradients $\check{\mathbf{F}} = \mathbf{PFP}$, it naturally arises as a plane tensor.

3 Speckle Tracking Echocardiography

Speckle tracking echocardiography (STE) is an application of pattern-matching technology to ultrasound cine data and is based on the tracking of the 'speckles' in a 2D plane or in a 3D volume (2DSTE and 3DSTE, respectively). Speckles are disturbances in ultrasounds caused by reflections in the ultrasound beam: each structure
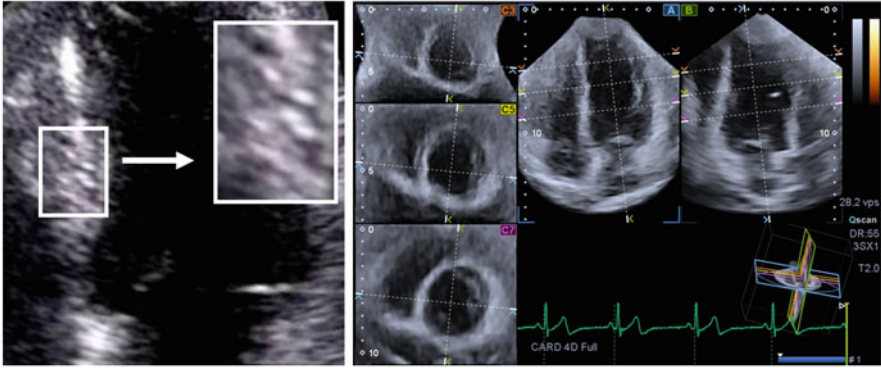
Fig. 2 Speckles moving with tissue as viewed through STE (*left*); the apical four chamber view (*A*); the second apical view orthogonal to plane A (*B*); three short-axis planes (*C*), in the apical region (*C1*), in the mid-ventricle (*C2*), and at the basal portion of the LV (C3) (*right*) (unmodified from the original ARTIDA image)

in the body has a unique speckle pattern that moves with tissue (Fig. 2, left panel). A square or cubic template image is created using a local myocardial region in the starting frame of the image data. The size of the template image is around 1 cm^2 in 2D or 1 cm^3 in 3D. In the successive frame, the algorithm identifies the local speckle pattern that most closely matches the template (see [29] for further details). A displacement vector is created using the location of the template and the matching image in the subsequent frame. Multiple templates can be used to observe displacements of the entire myocardium. By using hundreds of these samples in a single image, it is possible to provide regional information on the displacement of the LV walls, and thus, other parameters such as strain, rotation, twist and torsion can be derived.

Echocardiographic examinations were performed with an Aplio-Artida ultrasound system (Toshiba Medical Systems Co, Tochigi, Japan). Full-volume ECG-gated 3D data sets were acquired from apical positions using a 1–4 MHz 3D matrix array transducer to visualize the entire LV in a volumetric image. To obtain these 3D data sets, four or six sectors were scanned from consecutive cardiac cycles and combined to provide a larger pyramidal volume covering the entire LV. The final LV geometry was reconstructed by starting from a set of 6 homologous landmarks (see Fig. 2), manually detected by the operator for all subjects under study. The manual detection for a given set of landmarks is crucial because it allows recording spatial coordinates in perfectly comparable anatomical structures of different subjects (following a homology principle). The results of our 3DSTE system is a time-sequence of shapes, each constituted by 1297 landmarks, assumed to be homologous, for both the epicardial and endocardial surfaces, positioned along 36 horizontal circles, each comprised of 36 landmarks, plus the apex (see Fig. 3).

Typically, the results of the 3D-wall motion analysis are presented to the user as averaged values for each segment identified by the device according to the American
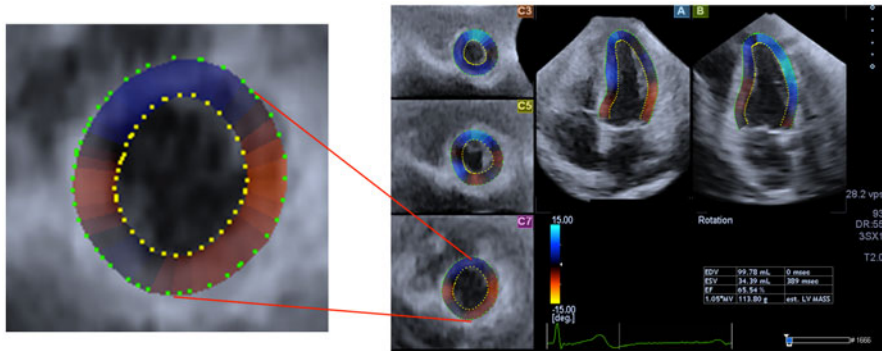
Fig. 3 The markers automatically set by the software supporting 3DSTE are shown as small yellow points on both three planes taken perpendicularly to the LV axis (*left panel*) and on two vertical sections (*right panel*). In particular, in the figure the color code corresponds to the torsional rotation of the LV at the beginning of the cardiac cycle (as evidenced by the small bar at the right bottom corner of the figure)

Heart Association standards for myocardial segmentation [2]: 6 basal segments (basal anterior (BA), basal antero-septum (BAS), basal infero-septum (BS), basal inferior (BI), basal posterior (BP), basal lateral (BL)); 6 middle segments (middle anterior (MA), middle antero-septum (MAS), middle infero-septum (MS), middle inferior (MI), middle posterior (MP), middle lateral (ML)); 4 apical segments (apical anterior (AA), apical septal (AS), apical inferior (AI), apical lateral (AL)). Hence, in each frame of the cardiac cycle time-curves graphs are generated, showing the mean values over the six middle segments, as the ones shown in Fig. 4, and representing the mean circumferential strains at any time along the cardiac cycle on each middle segment, and the overall mean value over the left ventricle's middle part, for a human subject.

3.1 Speckle Tracking Echocardiographic Data

In our case, it was possible to obtain the landmark clouds (upon which the standard rotational, torsional and strain parameters are computed and outputted by each Artida machine) by an unlocked version of the software equipping our PST25SX Artida device, thanks to a special opportunity provided in the context of an official research and development agreement between the Dipartimento di Scienze Cardiovascolari, Respiratorie, Nefrologiche Anestesiologiche e Geriatriche (Sapienza Università di Roma) and Toshiba Medical System Europe (Zoetermeer, The Netherland).

Our 3DSTE data were based on the acquisition made on a group of volunteers, who were randomly selected from the local list of employees at a single University Hospital Department. Individuals were subjectively healthy without a history of hypertension or cardiac disease and were not taking medications. They all had normal ECG and blood pressure below 140/90 mmHg [25]. Being the aim of the present
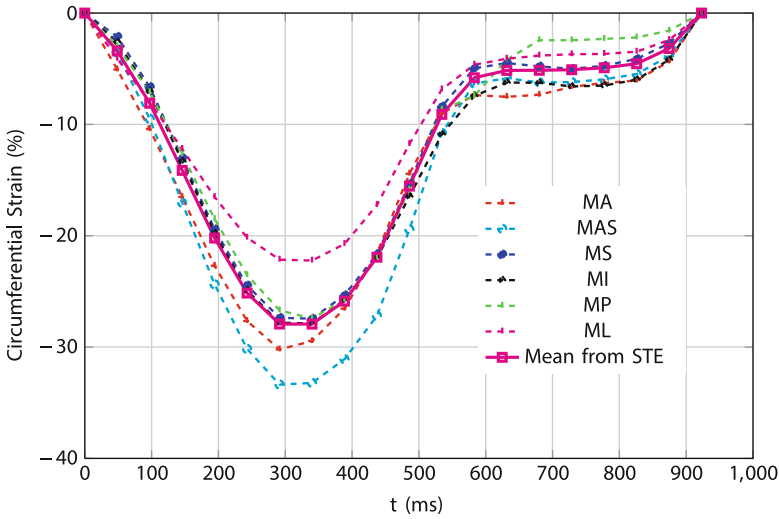
Fig. 4 Circumferential strains versus time: mean values of the circumferential strains on the six segments of the mid-myocardium identified by their acronyms (MA for middle-anterior, MAS for middle antero-septum, MS for middle infero-septum, MI for middle inferior, MP for middle posterior, ML for middle lateral); (*dashed* lines); mean value at mid-myocardium (solid, magenta)

work the analysis of the primary and secondary strain-line patterns in the LV walls, rough data from 3DSTE are played through MatLab, as prescribed by the protocol of measurement proposed and tested in [8], and shortly summed up in the next section.

3.2 MatLab Post-Processing Code

Starting from 3DSTE data on walls's motion and using the protocol proposed and verified in [8], the surface nonlinear strain tensor **C** on the LV epicardium and endocardium can be evaluated. Precisely, **C** is evaluated in correspondence of the landmarks (see Fig. 3), at each time along the cardiac cycle.

As already written, the real LV is identified by a cloud of $36 \times 36 \times 2 + 1$ points (called markers p_i) whose motion is followed along the cardiac cycle: the position of each of the $(36 \times 36) \times 2$ points p_i ($i = 1, 36 \times 36 \times 2$) is registered by the device at each time frame j of the cardiac cycle, and represented through the set of its Cartesian coordinates. These coordinates refer to a system represented by the $\mathbf{i}_3$ axis defined by the longitudinal LV axis and the $(\mathbf{i}_1, \mathbf{i}_2)$ axes on the orthogonal planes. The clouds of markers are intrinsically ordered. Figure 5 shows the endocardial (left panel) and epicardial (right panel) clouds $\mathcal{S}_{endo}$ and $\mathcal{S}_{epi}$ of points corresponding to our representative individual within the sample survey. To each point $P \in \mathcal{S}_{endo}$ ($\mathcal{S}_{epi}$), identified within the intrinsic reference system by the pairs of 3DSTE coordinates z and ϕ, corresponds a set of n positions within the Cartesian coordinate system, where
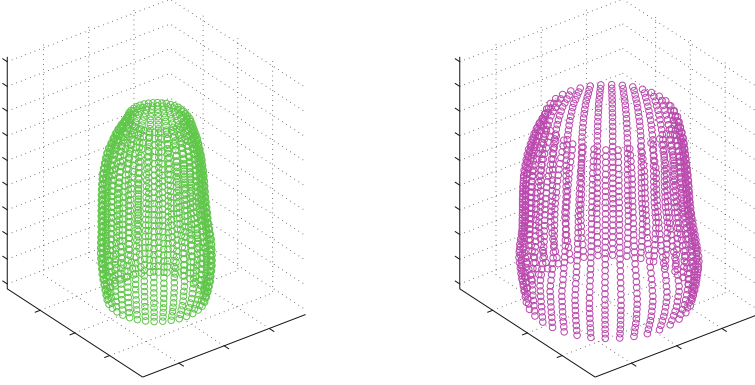
Fig. 5 Cloud of 1296 points automatically identified by the software on the endocardial (*left* panel, green empty dots) and epicardial (*right* panel, violet empty dots) surface, so as rendered by MatLab for a human subject within our group

n is the number of equally spaced frames registered by the device along the cardiac cycle. Moreover, let $P_z \in \mathcal{S}_{endo}$ and $P_\phi \in \mathcal{S}_{endo}$ be the points close to the point P in the 3DSTE topology, *i.e.* identified within the intrinsic reference system by the pair $(z + h_z, \phi)$ and $(z, \phi + h_\phi)$ of 3DSTE coordinates, where $h_z = H(LV)/36$, $h_\phi = 2\pi/10$, and $H(LV)$ the height of the LV model. The vectors $P_z - P$ and $P_\phi - P$ span a non-orthonormal covariant basis $(\mathbf{a}_1, \mathbf{a}_2)$ which corresponds to the 3DSTE coordinate system. The corresponding controvariant basis $(\mathbf{a}^1, \mathbf{a}^2)$ can be easily evaluated. Let p, p_z, and p_ϕ denote the positions occupied by the points P, P_z, and P_ϕ respectively at the frame j; they define the covariant basis $\tilde{\mathbf{a}}_1 = p_z - p$ and $\tilde{\mathbf{a}}_2 = (p_\phi - p)$.

Both $\mathbf{a}_\alpha$ and $\tilde{\mathbf{a}}_\alpha$ are known in terms of their Cartesian coordinates. Thus, the following holds:

$$\tilde{\mathbf{a}}_1 = \lambda_i^z(j)\,\mathbf{i}_i \quad \text{and} \quad \tilde{\mathbf{a}}_2 = \lambda_i^\phi(j)\,\mathbf{i}_i, \tag{3}$$

where j refers to the frame along the cardiac cycle;

$$\mathbf{a}_1 = \lambda_i^z\,\mathbf{i}_i \quad \text{and} \quad \mathbf{a}_2 = \lambda_i^\phi\,\mathbf{i}_i, \tag{4}$$
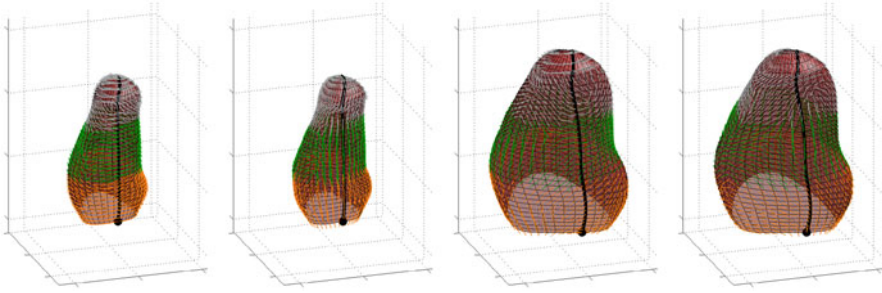
where $\lambda_i^\phi = \lambda_i^\phi(0)$ and $\lambda_i^z = \lambda_i^z(0)$.

At each point, the nonlinear strain tensor $\mathbf{C}$ can be evaluated through its components

$$\mathbf{C}_{\beta\delta} = \mathbf{F}^\alpha_\beta \, \mathbf{F}^\gamma_\delta \, (\mathbf{a}_\alpha \cdot \mathbf{a}_\gamma), \quad \alpha, \beta = 1, 2, \tag{5}$$

with

$$\mathbf{F}^\alpha_\beta = \mathbf{F}\,\mathbf{a}_\beta \cdot \mathbf{a}^\alpha = \tilde{\mathbf{a}}_\beta \cdot \mathbf{a}^\alpha. \tag{6}$$
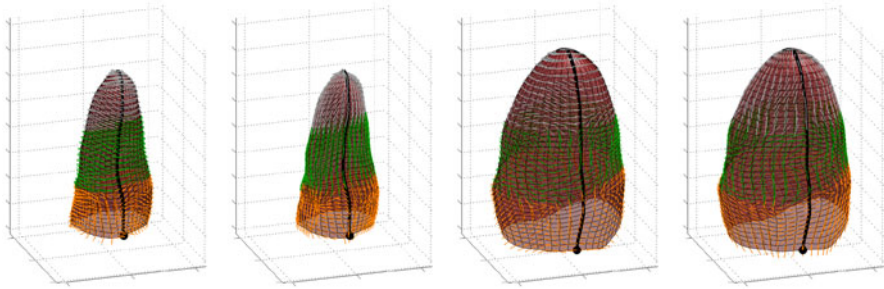
Fig. 6 Representation, in one subject, of the endocardial primary and secondary strain lines (from *left* to *right*: panel 1 and 2); and of the epicardial primary and secondary strain lines (from *left* to *right*: panel 3 and 4). It can be appreciated the behavior of primary strain lines in the middle (*green*) part of the LV

The eigenvalue analysis on **C** reveals a plane strain state, thus delivering the expected results concerning the primary and secondary strain lines. The corresponding eigenvalue-eigenvector pairs are denoted as $(\bar{\gamma}_\alpha, \bar{\mathbf{c}}_\alpha)$, where $\alpha = 2, 3$.

4   Principal Strain Lines in Real Human Left Ventricle

Through the protocol shortly summed up in the previous section, we can evaluate PSLs corresponding to different subjects. We started with the evaluation of primary and secondary strains and strain lines at the systolic peak. As cardiac cycle's duration is different from subject to subject, we needed at first to fix a few points along the cardiac cycle identifying homologous times, that is, times corresponding to the occurrences of special mechanical and electrical events which can be identified along any cardiac cycles. With this, we associate to the real-time scale based on the finite number of times caught by the 3DSTE device along the cardiac cycle, a new time scale, based on 6 homologous times which are the same along any cardiac cycle. The systolic time was identified as the one corresponding to the end systolic volume. Other homologous times before the systolic one are those corresponding to the peak of R wave and to the end of T wave; homologous times after the systolic one are those corresponding to the mitral-valve opening, to the end of rapid filling (beginning of diastasis), and to the onset of Q wave.

Figures 6 and 7 show endocardial and epicardial primary and secondary strain lines corresponding to the homologous systolic times and to two different human LVs, chosen among our data as representative of the group. The colors identify different parts of the LVs: grey for the apical part, green for the middle part, and orange for the basal part. Each line identifies the direction of the primary and secondary strain line at a point of the endocardial and epicardial cloud defined by 3DSTE. The endocardial and epicardial surfaces which in the figure represent the support for the strain lines correspond to the images of those surfaces at the systolic time.

Fig. 7 Representation, in another subject, of the endocardial primary and secondary strain lines (from *left* to *right*: panel 1 and 2); and of the epicardial primary and secondary strain lines (from *left* to *right*: panel 3 and 4). It can be appreciated the behavior of primary strain lines in the middle (*green*) part of the LV

As Figs. 6 and 7 show, the LV endocardial primary strain lines (first panel from left to right in both figures) have the same circumferential pattern evidenced in the model we studied in [8], even if in the basal part of the LV, the influence of the stiffer structure of the mitral annulus alter the circumferential pattern. Even if volumes and shapes are different one from another, endocardial primary strain lines are almost the same and circumferential. The first and second panels (from left to right) in both Figs. 6 and 7 are referred to the endocardial primary and secondary strain lines, which appear prevalently longitudinal in the middle part of the ventricle, according to the prevalent circumferential orientation of the primary strain lines there. The third and fourth panels show instead epicardial primary and secondary strain lines. The pattern of primary strain lines is less regular, even over the middle part of the ventricle, which should not be much influenced by the stiffer structure of the mitral annulus. However, in both cases, different zones are evident where epicardial primary strain lines follow lines which resemble muscle fiber directions. The results we got from our investigations, even if they need be supported by further data, allowed us to make a conjecture based on the pattern of endocardial primary strain lines. We conjecture that the inflation-induced dilation due to blood pressure is more effective for subendocardial layers, which dilating reduce the circumferential shortening induced by muscle contraction. Better is the capacity of the elastic response of the endocardial surface, smaller is the dilation induced by blood pressure.

It means that the capacity to contrast blood pressure is reduced in patients with volume overload, hence the primary strain values which correspond to the circumferential principal strain lines are smaller It follows that the behavior of primary strain lines when special remodeling effects take place in the left ventricle, due to the onset of cardiac pathologies is one of our future objectives [21].

Importantly, the noninvasive analysis of this kind of data may be easily supported within a 3DSTE device, through the post-processing method we proposed in [8] and shortly summed up here. As an example, and with reference to the same human subject whose 3DSTE circumferential strain were shown in Fig. 4, we pictured in Fig. 8, the endocardial and epicardial mean values, taken over the middle part of the
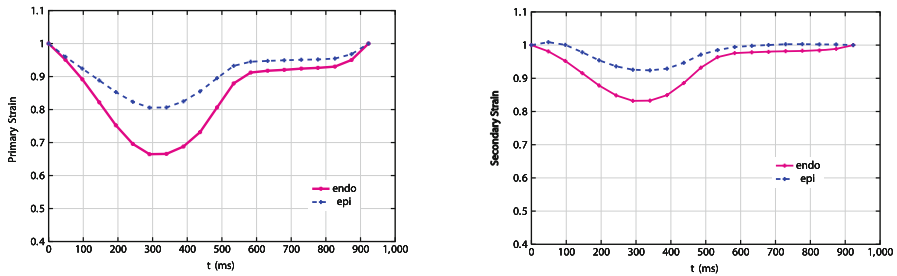
Fig. 8 Representation of the pattern of the mean values, over the middle part of the left ventricle, of the primary (*left panel*) and secondary (*right panel*) epicardial and endocardial strains along the cardiac cycle

left ventricle, of the primary and secondary strains. It might be possible to infer from a large scale investigation appropriate confidence intervals for these values, when referred to healthy situations.

References

1. Burkhoff D, Mirsky I, Suga H (2005) Assessment of systolic and diastolic ventricular properties via pressure-volume analysis: a guide for clinical, translational, and basic researchers. AJP-Heart 289:501–512
2. Cerqueira MD, Weissman NJ, Dilsizian V, Jacobs AK, Kaul S, Laskey WK, Pennel DJ, Rumberger JA, Ryan T, Verani MS (2002) Standardized myocardial segmentation and nomenclature for tomographic imaging of the heart: a statement for healthcare professionals from the Cardiac Imaging Committee of the Council on Clinical Cardiology of the American Heart Association. Circulation 105:539–542
3. DeAnda A, Komeda M, Nikolic SD, Daughters GT, Ingels NB, Miller DC (1995) Left ventricular function, twist, and recoil after mitral valve replacement. Circulation 92:458–466
4. Evangelista A, Nesser J, De Castro S, Faletra F, Kuvin J, Patel A, Alsheikh-Ali AA, Pandian N (2009) Systolic wringing of the left ventricular myocardium: characterization of myocardial rotation and twist in endocardial and midmyocardial layers in normal humans employing three-dimensional speckle tracking study. (Abstract) J Am Coll Cardiol 53(A239):1018–268
5. Evangelista A, Nardinocchi P, Puddu PE, Teresi L, Torromeo C, Varano V (2011) Torsion of the human left ventricle: experimental analysis and computational modelling. Prog Biophys Mol Biol 107(1):112–121
6. Evangelista A, Gabriele S, Nardinocchi Piras P, Puddu PE, Teresi L, Torromeo C, Varano V (2015) On the strain-line pattern in the real human left ventricle. J Biomech. doi:10.1016/j.jbiomech.2014.12.028. published on line: 15 Dec 2015

7. Evangelista A, Gabriele S, Nardinocchi P, Piras P, Puddu PE, Teresi L, Torromeo C, Varano V (2014) A comparative analysis of the strain-line pattern in the human left ventricle: experiments vs modeling. Comput Method Biomech Biomed Eng Imaging Vis. doi:10.1080/21681163.2014.927741. Published online: 23 Jun 2014

8. Fung YC (1993). Biomechanics, 2nd edn. Springer, New–York

9. Gabriele S, Nardinocchi P, Varano V (2015) Evaluation of the strain-line patterns in a human left ventricle: a simulation study. Computer Methods in Biomechanics and Biomedical Engineering 18(7), 790–798.

10. Gabriele S, Teresi L, Varano V, Evangelista A, Nardinocchi P, Puddu PE, Torromeo C (2014) On the strain line patterns in a real human left ventricle. In: Tavares JMRS, Jorge RMN (eds) Computational vision and medical image processing IV. CRC Press, Boca Raton

11. Geyer H, Caracciolo G, Abe H, Wilansky S, Carerj S, Gentile F, Nesser HJ, Khandheria B, Narula J, Sengupta PP (2010) Assessment of myocardial mechanics using speckle tracking echocardiography: fundamentals and clinical applications. J Am Soc Echo 23:351–369

12. Goffinet C, Chenot F, Robert A, Pouleur AC, le Polain de Waroux JB, Vancrayenest D, Gerard O, Pasquet A, Gerber BL, Vanoverschelde JL (2009) Assessment of subendocardial vs. subepicardial left ventricular rotation and twist using two dimensional speckle tracking echocardiography comparison with tagged cardiac magnetic resonance. Eur Heart J 30:608–617

13. Helle–Valle T, Crosby J, Edvardsen T, Lyseggen E, Amundsen BH, Smith HJ, Rosen BD, Lima JAC, Torp H, Ihlen H, Smiseth OA (2005) New noninvasive method for assessment of left ventricular rotation: speckle tracking echocardiography. Circulation 112:3149–3156

14. Helle–Valle T, Remme EW, Lyseggen E, Petersen E, Vartdal T, Opdahl A, Smith HJ, Osman NF, Ihlen H, Edvardsen T, Smiseth OA (2009) Clinical assessment of left ventricular rotation and strain: a novel approach for quantification of function in infarcted myocardium and its border zones. Am J Physiol Heart Circ Physiol 297:H257–H267

15. Nash MP, Hunter PJ (2000) Computational mechanics of the heart: from tissue structure to ventricular function. J Elast. 61:113–141

16. Humphrey JD (2002) Cardiovascular solid mechanics: cells, tissues, organs. Springer, New York

17. Maffessanti F, Nesser HJ, Weinert L, Steringer–Mascherbauer R, Niel J, Gorissend W, Sugeng L, Lang RM, Mor–Avi V (2009) Quantitative evaluation of regional left ventricular function using three-dimensional speckle tracking echocardiography in patients with and without heart disease. Am J Cardiol 104:1755–1762

18. Mangual JO, De Luca A, Toncelli L, Domenichini F, Galanti G, Pedrizzetti G (2012) Three–dimensional reconstruction of the functional strain–line patterns in the left ventricle from 3-dimensional echocardiography. Circ Cardiovasc Imaging 5:808–809

19. Nagel E, Stuber M, Burkhard B, Fischer SE, Scheidegger MB, Boesiger P, Hess OM (2000) Cardiac rotation and relaxation in patients with aortic valve stenosis. Eur Heart J 21:582–589

20. Pedrizzetti G, Kraigher-Krainer E, De Luca A, Caracciolo G, Mangual JO, Shah A, Toncelli L, Domenichini F, Tonti G, Galanti G, Sengupta PP, Narula J, Solomon S (2012) Functional strain-line pattern in the human left ventricle. PRL 109:048103

21. Piras P, Evangelista A, Gabriele S, Nardinocchi P, Teresi L, Torromeo C, Varano V, Puddu PE (2014) 4D-analysis of left ventricular cycle in healthy subjects using procrustes motion analysis. PlosOne 9: e86896

22. Rüssel IK, Götte MJW, Bronzwaer JC, Knaapen P, Paulus WJ, van Rossum AC (2009) Left ventricular torsion. An expanding role in the analysis of myocardial dysfunction. JACC 2(5):648–655

23. Shaw SM, Fox DJ, Williams SG (2008) The development of left ventricular torsion and its clinical relevance. Int J Cardiol 130:319–325

24. Tibayan FA, Lai DT, Timek TA, Dagum P, Liang D, Daughters GT, Ingels NB, Miller DC (2002) Alterations in left ventricular torsion in tachycardia–induced dilated cardiomyopathy. J Thorac Cardiovasc Surg 124(1):43–49

25. Torromeo C, Evangelista A, Pandian NG, Nardinocchi P, Varano V, Gabriele S, Schiariti M, Teresi L, Piras P, Puddu PE (2014) Torsional correlates for end systolic volume index in adult healthy subjects. Int J Appl Sci Technol 4(4):11–23.
26. Waldman LK, Fung YC, Covell JW (1985) Transmural myocardial deformation in the canine left ventricle. Normal in vivo three-dimensional finite strains. Circ Res 57:152–163
27. Wang VY, Hoogendoorn C, Frangi AF, Cowan BR, Hunter PJ, Young AA, Nash MP (2013) Automated personalised human left ventricular FE models to investigate heart failure mechanics. In: Camara et al. (eds) Statistical atlases and computational models of the heart. Imaging and modelling challenges. Lecture Notes in Computer Science, vol 7746, pp 307–316
28. Weiner RB, Hutter AM, Wang F, Kim J, Weyman AE, Wood MJ, Picard MH, Baggish AL (2010) The impact of endurance exercise training on left ventricular torsion. J Am Coll Cardiol Img 3:1001–1009
29. Yeung F, Levinson SF, Parker KJ (1998) Multilevel and motion model-based ultrasonic speckle tracking algorithms. Ultrasound Med Biol 24:427–441